PROCEEDINGS OF SCIENCE

Unveiling the seasonal variation of multi-muon events at the NOνA Detector

Jordi Tuneu,[a,*] **Eva Santos**[a] **and Peter Filip**[a]

[a] *FZU - Institute of Physics of the Czech Academy of Sciences, Na Slovance 1, Prague, Czech Republic*

E-mail: tuneu@fzu.cz, esantos@fzu.cz, filip@fzu.cz

In this contribution, we investigate the seasonal variation of multi-muon events observed by the NOνA Near Detector (ND) at Fermilab, using the general-purpose Monte Carlo code FLUKA-CERN to simulate the transport and interaction of the air-shower particles in the atmosphere and other media. Our atmospheric model uses air densities for Winter and Summer averaged profiles calculated from the temperature and geopotential information at 37 pressure levels given by the European Center for Medium-Range Weather Forecasts (ECMWF) datasets in situ. Our FLUKA geometry model also includes a layered underground approximated to match the NOνA ND and its location. We compare our simulation results with the measured seasonal flux modulation of multi-muon events by the NOνA ND. For the first time, we were able to describe the multi-muon excess in Winter over Summer quantitatively and the dependence on the multi-muon event multiplicity as observed by NOνA. Finally, we compare our results for the muon flux at the surface and detector level obtained from FLUKA simulations with the previous work from other authors based on CORSIKA simulations. We try to understand the reasons for the discrepancy by nearly a factor of four between the results of two Monte Carlo codes.

The 38th International Cosmic Ray Conference (ICRC2023)
26 July – 3 August, 2023
Nagoya, Japan

*Speaker

PoS(ICRC2023)347

1. Introduction

Due to temperature changes along the year, the atmospheric profiles undergo seasonal variations affecting the height of the first interaction of cosmic rays, from which a seasonal variation of the muon fluxes is also expected. The maximum amplitude of this modulation is expected to occur when comparing Winter to Summer months. The MINOS and NOνA near detectors (NDs) located 99 m underground [1, 2] have studied this modulation. MINOS cosmic data [3] show that the total (single)-muon flux increases in Summer and decreases in Winter by $\approx$ 1%. In contrast, both experiments [1, 2] find the multi-muon event rates to reach a maximum during Winter and a minimum in the Summer. The magnitude of the seasonal multi-muon flux oscillation is five times larger than the one for single-muons, and it has an opposite phase: the maximum is shifted by approximately six months. In [2], the MINOS Collaboration has proposed several mechanisms to explain the Winter maximum for the observed multi-muon flux. However, all of them fell short of describing the magnitude of the oscillation. A recent work [4] using CORSIKA [5] simulations has also addressed this issue. Still, a quantitative agreement was not obtained: the predicted seasonal multi-muon oscillation magnitude (see [4], Figure 9) is four times smaller than in the MINOS and NOνA data, showing that even in the well-known TeV range, discrepancies between data and Monte Carlo simulations exist. A proper understanding of this problem could help improve existing Monte Carlo codes or even hint at new physics processes in hadronic interactions.

In this work, we use the general-purpose Monte Carlo code FLUKA-CERN [6] to treat the transport and interaction of shower particles in the atmosphere and other media. In particular, we have used the 100-layered atmospheric model from FLUKA, for which we have calculated the averaged air density of the Summer and Winter profiles from the ECMWF data [7] at the NOνA/MINOS NDs location for the two-year period of the NOνA data taking. The muon component was analyzed at the surface (226 m above sea level) and at the detector plane (99 m underground) for both atmospheric profiles. The atmospheric model and geometry layout are described in section 2. Results are discussed in section 3. A summary of our results is given in section 4.

2. Atmospheric Model and Detector Geometry

Our atmospheric model is based on the 100-layered atmospheric model from FLUKA [8], adapted for the NOνA ND geometry and location, considering different atmospheric profiles for Winter and Summer. Since we only consider cosmic rays with zenith angles below 70° reaching a $\approx$ 20 km $\times$ 20 km surface area, reducing to a $\approx$ 2 km $\times$ 2 km area at the detector plane, we have neglected the effects of the curvature of the Earth. Our FLUKA model was changed to a cylindrical geometry instead of the one from the original model. The full detector layout includes four underground layers, allowing for proper treatment of the interaction and propagation of the muons. The description of our atmosphere starts at 72 km altitude, with a density of 8.78×10^{-8} g cm^{-3} for both atmospheric profiles. The air density gradually increases over the one hundred layers, reaching 1.21×10^{-3} g cm^{-3} and 1.28×10^{-3} g cm^{-3} at the surface (226 m a.s.l.) for the Summer and Winter profiles, respectively. The air densities for the Winter and Summer profiles have been calculated from the temperatures and geopotential information for 37 pressure levels given by the ERA5 ECMWF [7] dataset in situ (averaged data from January and July 2017 periods were used). We have implemented a simple uniform magnetic field permeating the whole cylindrical volume with components $B_x[\mu\text{T}] = 19.3$, $B_y[\mu\text{T}] = 0$, and $B_z[\mu\text{T}] = 49.7$, using the IGRF2020 model,

defined for the Fermilab site coordinates in 2017 according to [9]. The first underground layer has a thickness of 99 m, ranging from the surface level down to an altitude of 127 m a.s.l., where the NOνA ND experiment is installed. It has a molasse composition with a density of 2.35 g cm^{-3}. At this depth, we implement the second underground layer, which consists of a cavity of 2 m height filled with air, with a density of 1.205×10^{-3} g cm^{-3}. The end of the second layer coincides with the altitude of the top of the NOνA detector, at 125 m a.s.l., followed by a four meters layer of mineral oil (1 g cm^{-3}). Finally, we add a molasse layer that reaches the sea level, which further slows down and absorbs the particles, as illustrated in Figure 1.

2.1 FLUKA cosmic-ray shower library

For the work presented in this paper, we have used the Monte Carlo code FLUKA-CERN [6], version 4-2.3, with the hadronic interaction model DPMJET [10].

Muons require a minimum energy of about 50 GeV to reach the NOνA ND, increasing to $\approx$ 200 GeV for more inclined air showers. The bulk of the muons seen by the NOνA ND is located within less than 500 m from the shower core [11]. We assume that muons have high rigidities at such energies and propagate in straight lines nearly parallel to the shower axis, preserving the zenith-angle distribution of the incoming cosmic rays. Therefore, we simulate cosmic rays arriving at the zenith-angle range θ = 15° to 60°, using a bin size of 5°.

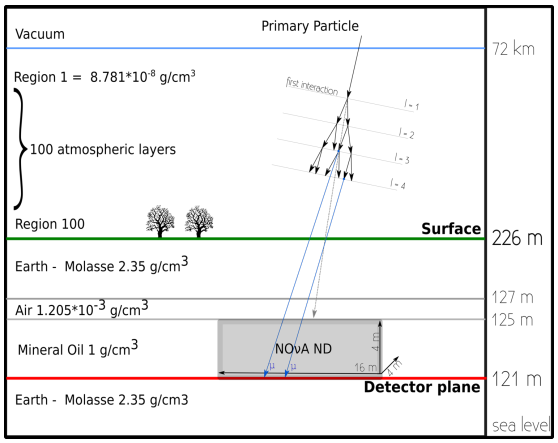

Figure 1: Sketch of the FLUKA full detector geometry layout. The drawing is not to scale.

We adjust the position of the incident cosmic ray so that the shower axis intersects the ground at coordinates $x = y = z = 0$. The full zenith angle distribution follows the NOνA ND acceptance, according to [1]. The energy distribution ranges from $E_{\rm min}$ = 10 TeV to $E_{\rm max}$ = 1 PeV, following a power-law distribution with spectral index γ = 2.7. We consider a four-component cosmic-ray mass composition with fractions according to the Global Spline Fit (GSF) model [12] over the whole energy range (see Figure 2). Specifically, we use the ratios at $\approx$ 15TeV: p/He = 1, p/CNO = 2.3, and p/Fe = 4.3. We have used Nitrogen for the CNO group. There are roughly 2×10^5 showers per season, from which we randomly select a sample of $\approx 1.35\times10^5$ (and $\approx 1.16\times10^5$) showers for $15° < \theta < 60°$ (and $20° < \theta < 60°$).

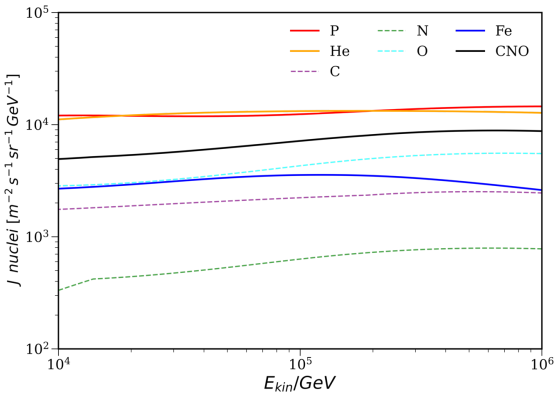

Figure 2: Cosmic-ray fluxes of p, He, C, N, O, Fe, and CNO primaries according to Global Spine Fit model [12] in the 10 TeV to 1 PeV energy range.

Our results are discussed in section 3. The shower fraction used per elemental group is shown in Table 1.

3. Results

In this section, we report on our findings regarding the muon flux differences for the Winter and Summer atmospheres.

In section 3.1, we present our results on the multi-muon seasonal variation obtained from our FLUKA-CERN simulations and compare them to the NOνA ND observations, namely the amplitude of the seasonal variation of multi-muons and its multiplicity dependence. In section 3.2, we compare the FLUKA-CERN and CORSIKA predicted muon fluxes at the surface and the detector plane after applying Elbert's formula [13] for the muon propagation underground. We apply our multi-muons *spotter* algorithm at the detector plane and discuss the obtained results for the two Monte Carlo codes.

Table 1: Number of showers per zenith-angle bin used for each cosmic-ray primary species.

θ (deg)	p	He	CNO	Fe
15-20	6880	6880	2991	1600
20-25	8320	8320	3617	1935
25-30	8160	8160	3548	1898
30-35	7360	7360	3200	1712
35-40	6400	6400	2783	1488
40-45	4960	4960	2157	1153
45-50	3840	3840	1670	893
50-55	2720	2720	1183	633
55-60	1760	1760	765	409

For our analysis, we used the FLUKA-CERN shower library described in subsection 2.1 and a fixed energy and zenith angle library used in [11], from which we stored the information regarding the position and momenta of all muons produced along the shower development.

3.1 Multi-muons: Seasonal Variation

To reduce the statistical uncertainties in the analysis of multi-muon events in each shower, we have implemented a grid of virtual NOνA ND detectors of size 16×4 m over a 2 km^2 area of the detector plane, located between $|x| < 1000$ m, $|y| < 1000$ m. Each shower is evaluated using all 62500 detectors individually, counting the number of muons in each virtual detector. The resulting amplitude of the seasonal variation comes from the comparison of $\approx 1.35 \times 10^5$ (and $\approx 1.16 \times 10^5$) showers per each season for $15^\circ < \theta < 60^\circ$ (and $20^\circ < \theta < 60^\circ$) zenith angles, selected according to Table 1. The multi-muon measurements made by NOνA-ND [1] implement a cosine fit of the NOνA monthly data averaged over two years, given by:

$$f(t) = V_0 + V\cos(\omega t + \phi), \tag{1}$$

where $V_0 = 0 \pm 0.1\%$, $V = 4.1 \pm 0.2\%$, and $\phi = -0.43 \pm 0.05\%$. The value of the phase ϕ corresponds to a maximum multi-muon rate around January 25$^{\text{th}}$ and a minimum rate near July 26$^{\text{th}}$. We use this fit and the data points for the maximum amplitude $V(\%)$ obtained by NOνA and compare them to our results considering the total multi-muon flux and multiplicities M = 2, 3, 4, 5, and ≥ 6. Our simulated multi-muon flux for the January and July 2017 periods is shown in Figure 3a. For the angular distribution $\theta = 15^\circ - 60^\circ$ (orange points) and $\theta = 20^\circ - 60^\circ$ (blue points), obtaining $V = 3.39\%$ for the former and $V = 3.70\%$ for the latter. We present the multiplicity dependence obtained for $\theta = 20^\circ - 60^\circ$ simulation in Figure 3b, with an excellent trend regarding the NOνA fits (colored lines). The fit lines are given to guide the eye since the NOνA multiplicity-dependent observation [1] has large error bars for the higher multiplicities. Figure 4 suggests that the presence of heavier nuclei is relevant to explain the larger seasonal oscillation of the higher multi-muon multiplicity flux observed by the NOνA ND.

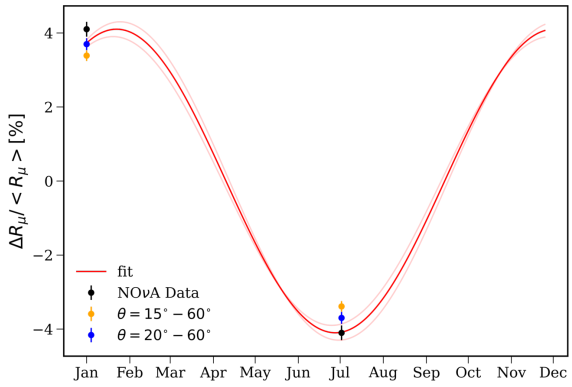

(a) Multi-muon flux seasonal variation obtained with FLUKA for the zenith angle range $\theta = 20°-60°$ (blue), and $\theta = 15° - 60°$ (orange). In black, two NOνA data points and the cosine fit (red line) obtained from two years of data by NOνA [1].

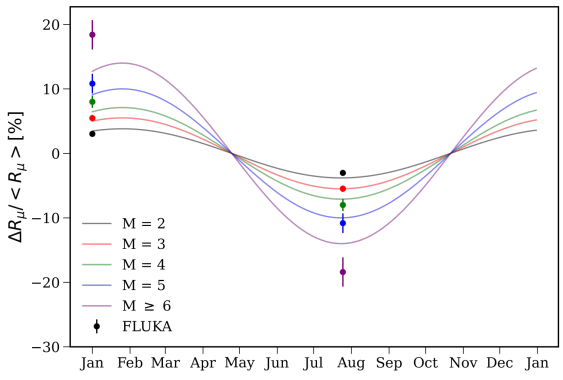

(b) Multi-muon flux seasonal variation obtained with FLUKA (colored points) for the multiplicities M = 2, 3, 4, 5 and ≥ 6 and the cosine fits (colored lines) obtained from the two years of NOνA data [1].

Figure 3: Seasonal variation for all multiplicities (left panel) and its multiplicity dependence (right panel).

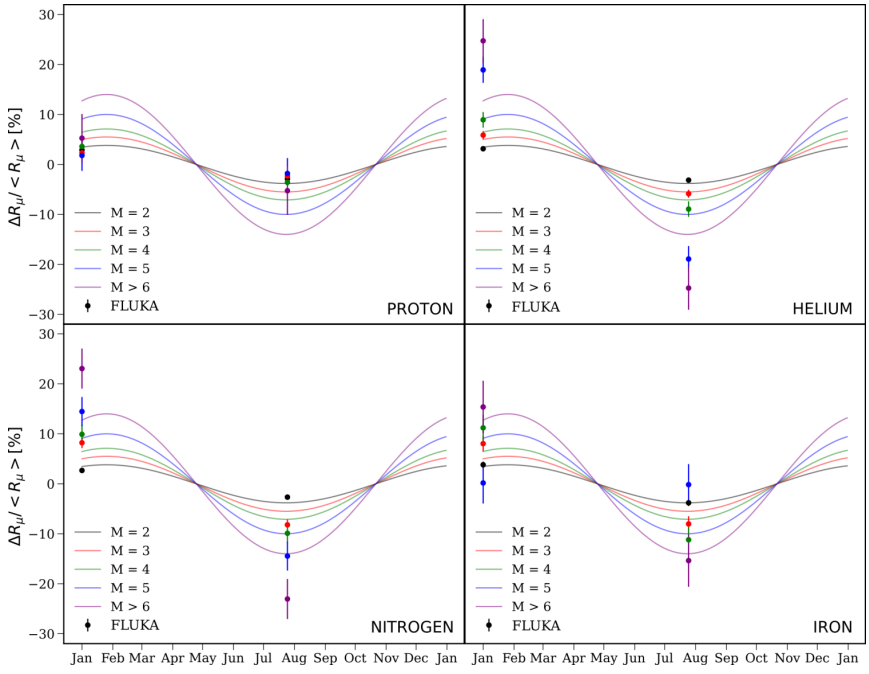

Figure 4: Multiplicity values of the multi-muon flux modulation for proton (p), helium (He), nitrogen (N), and iron (Fe) obtained with FLUKA (colored points) for the multiplicities M = 2, 3, 4, 5 and ≥ 6 and the cosine fits (colored lines) obtained from the two years of NOνA data [1]

Finally, we show the contribution of each primary particle species used in the simulations to the total multi-muon flux variation (see Figure 5). We find a multi-muon excess in Winter over Summer for each element, obtaining $V = 2.85\%$ for protons, 3.87% for helium, 4.25% for the CNO group, and 5.02% for iron, emphasizing the importance of the presence of heavier nuclei for achieving a total multi-muon seasonal variation comparable with the NOνA ND observations [1].

3.2 CORSIKA-FLUKA comparison

In this work, we have shown, for the first time, a good agreement between the seasonal multi-muon flux variation, measured by the MINOS and NOνA ND [1, 3], with FLUKA-CERN 4.2.3 [6] simulations. Our work was motivated by previous studies using CORSIKA simulations, or CORSIKA-based parametrizations, which could not properly describe the observed multi-muon seasonal flux modulation [3, 4]. To understand the origin of this discrepancy, we aim to compare FLUKA-CERN 4-2.2 [6] and CORSIKA 7.7500 [5] results regarding the muon content of extensive air showers. For a fair comparison between the two Monte Carlo codes, our CORSIKA 7.7500 simulations will be produced as closely as possible to the ones of FLUKA, described in [11]. For this purpose, we have compared 4000 (1000) proton-induced showers with 50 (100 TeV) primary energy at the fixed zenith angles θ = 0°, 30°, and 50°. For the CORSIKA simulations, we have used Sibyll 2.3d [14] as the high-energy hadronic interaction model to simulate hadronic interactions from the highest energies to 80 GeV. Below 80 GeV, elastic and inelastic cross-sections of hadrons in air, their interactions, and particle production are handled by FLUKA-INFN 2021.2.9 [15]. In Table 2, we show the quantity $\langle h_{s,w} \rangle$, i.e., the mean value of the height of the first interaction for the primary protons generated by both Monte Carlo codes for the Summer and Winter atmospheric profiles. We observe that, in general, the height of the first interaction slightly increases as a function of the zenith angle and primary energy. We also calculate the mean difference of the height of the first interaction for the Summer and Winter atmospheric profiles, $\Delta_{sw} = \langle h_s - h_w \rangle$. We notice that the differences between Summer and Winter are systematically higher in FLUKA (above 650 m) than in CORSIKA, which, in some cases, are remarkably small. The distribution of the height of the first interaction for 50 TeV (left panels) and 100 TeV (right panels) showers with θ = 30° are shown in Figure 6. The dashed lines represent the mean value of the distribution for each case. This result is relevant since the height of the first interaction is closely related to the shower development and the spatial distribution of muons at the ground level.

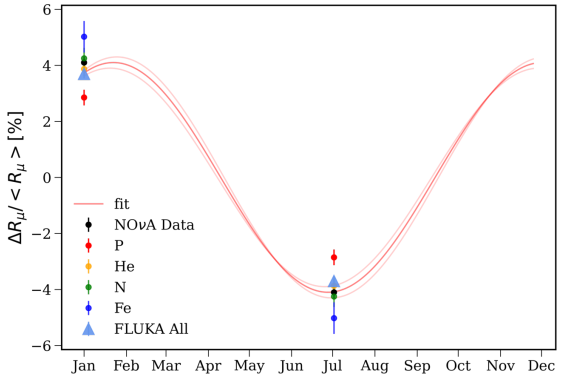

Figure 5: Contribution of protons (red), helium (orange), nitrogen (green) and iron (blue) for the seasonal variation. The light-blue triangle represents all the contributions together. The black point and red line are the NOνA data and the cosine fit for the averaged two years of observations.

Table 2: Average values of the height of the first interaction in Summer (s), Winter (w), and the shift between both (Δ_{sw}) for FLUKA and CORSIKA.

θ (deg)	E [TeV]	FLUKA			CORSIKA		
		$\langle h_s \rangle$ [km]	$\langle h_w \rangle$ [km]	Δ_{sw} [km]	$\langle h_s \rangle$ [km]	$\langle h_w \rangle$ [km]	Δ_{sw} [km]
0°	50	21.87	21.15	0.72	20.96	20.80	0.16
	100	22.47	21.31	1.16	21.34	20.96	0.38
30°	50	22.90	22.06	0.84	21.87	21.85	0.02
	100	22.72	21.96	0.76	22.52	22.52	0.00
50°	50	24.63	23.97	0.66	24.00	23.97	0.03
	100	25.29	23.96	1.33	24.59	24.40	0.19

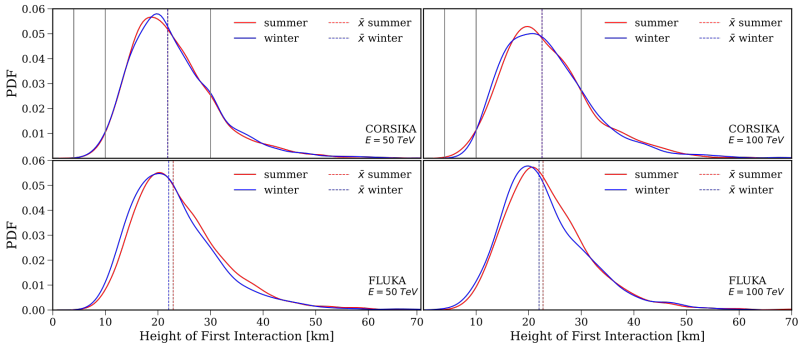

Figure 6: Distributions of the height of the first interaction for 50 TeV (left) and 100 TeV (right) proton-induced showers with $\theta = 30°$, for CORSIKA (top) and FLUKA (bottom). The dashed lines represent the mean of height of the first interaction for each season. The gray lines in the CORSIKA panels correspond to the height of the first four CORSIKA atmospheric layers at 4, 10, and 30 km.

The obtained results are similar for the remaining zenith angles of 0° and 50°. The lateral muon spatial distribution difference is a key factor for the number of multi-muons accounted for [11]. In particular, for 50 TeV showers at 30°, we observe a difference in the standard deviations in the XY plane for Summer and Winter in FLUKA (CORSIKA) of $\Delta_x\sigma_{sw} = 15.46$ m, $\Delta_y\sigma_{sw} = 11.62$ m ($\Delta_x\sigma_{sw} = 0.08$ m, $\Delta_y\sigma_{sw} = 5.70$ m).

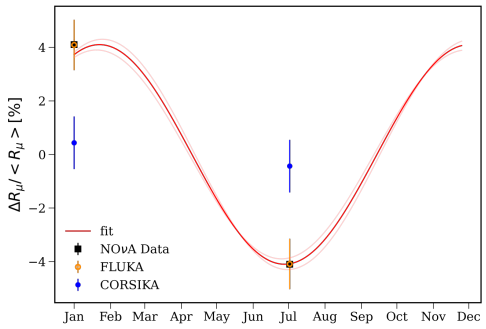

Figure 7: Multi-muon seasonal flux amplitude for CORSIKA (blue), and FLUKA (orange) 50 TeV showers, $\theta = 30°$. The black square and the red line are the NOνA data and the cosine fit for the averaged two years of observations.

While FLUKA can be used to simulate the particle transport from the top of the atmosphere to the detector plane in several media, CORSIKA can only be used to simulate the shower development in the Earth's atmosphere. To account for the number of multi-muons at the detector plane, we have considered the muons generated by the two Monte Carlo codes at the surface, and we have applied a cut according to Elbert's equation [13].

This way, we avoid systematic differences between both codes due to the transport of muons underground. We have applied an energy cut of 50 GeV for muons produced in showers with $\theta = 0°$, 55 GeV for $\theta = 30°$, and 75 GeV for $\theta = 50°$. To estimate the number of multi-muons, we have followed the same procedure described in section 3.1 for all the FLUKA and CORSIKA showers. In Figure 7, we show the result of sea-

Table 3: FLUKA and CORSIKA amplitudes of the seasonal multi-muon flux modulation.

θ	E [TeV]	V [%] FLUKA	V [%] CORSIKA
0°	50	3.75 ± 0.76	1.75 ± 0.76
	100	2.24 ± 0.91	0.39 ± 0.92
30°	50	4.09 ± 0.94	0.44 ± 0.98
	100	4.10 ± 1.08	0.55 ± 1.14
50°	50	4.96 ± 1.70	3.01 ± 1.87
	100	3.11 ± 1.92	0.59 ± 2.06

sonal variation for $\theta = 30°$ and $E = 50$ TeV proton-initiated showers. We observe a $V = 4.09 \pm 0.98\%$ ($V = 0.44 \pm 0.94\%$) in FLUKA (CORSIKA). In Table 3, we summarize the obtained seasonal variations for each zenith angle and primary energy. Note that the muon energy cut used by the highest zenith angle directly affects the statistics producing larger error bars since fewer muons survive the energy cut.

4. Summary

- We are able to reproduce quantitatively the multi-muon excess in Winter over Summer observed by the NOνA and MINOS Near Detectors at FNAL, using the FLUKA simulations.
- We also describe the multiplicity-dependence of the multi-muon seasonal oscillation amplitude, and we point out that the contribution of heavy primaries is essential for this behavior.
- CORSIKA simulations, based on a five-layered atmosphere, fail to generate a significant difference in the multi-muon flux for Summer and Winter, which also applies to the difference of the first interaction height of protons.
- FLUKA simulations show a significant seasonal difference (between 0.6 and 1 km) for the first interaction height of protons, apparently due to the better description of the atmosphere.
- We suggest the description of the atmospheric density profile in the Monte Carlo codes seems to be critical for reproducing the seasonal variations observed by NOνA and MINOS.

Acknowledgments

This work is fully funded by the Czech Science Foundation under the project GAČR 21-02226M and by the project LM2023061 (FERMILAB-CZ) financially supported by the Ministry of Education, Youth, and Sports of the Czech Republic.

References

[1] Acero, M. A. *et al.*, [NOνA Collaboration], Phys. Rev. D, **99**, 122004 (2019).
[2] Adamson, P. *et al.*, [MINOS Collaboration], Phys. Rev. D, **91**, 112006 (2015).
[3] Adamson P. *et al.*, [MINOS Collaboration], Phys. Rev. D **90**, 012010 (2014).
[4] Gaisser, T. K. and Verpoest, S., Astropart. Phys., **133**, 102630 (2021).
[5] Heck, D., Capdevielle, J., Schatz, J. N., Schatz, G. and Thouw, T. Report FZKA **6019** (1998).
[6] Battistoni, G. *et al.*, Annals Nucl. Energy **82**, 10-18 (2015).
[7] "European Centre for Medium-Range Weather Forecasts": `https://www.ecmwf.int/`
[8] Battistoni, G., Margiotta, A., Muraro, S. and Sioli, M., Nucl. Instrum. Meth. A **626-627**, S191-S192 (2011).
[9] "National Oceanic and Atmospheric Administration": `https://www.ngdc.noaa.gov`
[10] Kling, A. *et al.*, Springer, Berlin, Heidelberg, (2001) 1033–1038.
[11] J. Tuneu, P. Filip, E. Santos EPJ Web Conf. **283** (2023), 05008.
[12] Dembinski, H. P., Engel, R., Fedynitch, A., Gaisser, T., Riehn, F. and Stanev, T., PoS **ICRC2017** (2018), 533.
[13] J. W. Elbert, Proceedings of the DUMAND Summer Workshop, La Jolla CA, USA (1979) 101–121;
J. W. Elbert, Proc. 16th ICRC 1979 Kyoto, Japan (1979), 405-409.
[14] F. Riehn, H. P. Dembinski, R. Engel, A. Fedynitch, T. K. Gaisser and T. Stanev, PoS **ICRC2017** (2018), 301;
F. Riehn, R. Engel, A. Fedynitch, T. K. Gaisser and T. Stanev, Phys. Rev. D **102** (2020) no.6, 063002.
[15] "FLUKA": `http://www.fluka.org/fluka.php`